The Role of Etching in the Formation of Ag Nanoplates with Straight, Curved and Wavy Edges and Comparison of Their SERS Properties

*Yin Yang, Xiao-Lan Zhong, Qiang Zhang, Logan G. Blackstad, Zheng-Wen Fu, Zhi-Yuan Li, and Dong Qin**

We investigate the role of etching in the formation of Ag nanoplates with different morphologies. By examining the reduction of $AgNO_3$ with poly(vinyl pyrrolidone) in an aqueous solution under a hydrothermal condition, we confirm that etching plays an essential role in promoting the growth of Ag triangular nanoplates with straight edges at the expense of multiple twinned particles via Ostwald ripening. Once all the multiple twinned particles are gone, etching will continue at the corners of nanoplates, leading to the formation of enneahedral nanoplates with curved edges. When the nanoplates with straight edges are transferred into ethanol and subjected to a solvothermal treatment, we obtain nanoplates with wavy edges and sharp corners due to etching on the edges. A comparison study indicates that, at the same particle concentration, Ag nanoplates with wavy edges embraces a SERS enhancement factor at least 6 and 13 times stronger than those with straight and curved edges, respectively. The results from finite difference time domain calculations support our experimental observation that the sharp features on nanoplates with wavy edges are the most active sites for SERS.

1. Introduction

Silver nanocrystals have fascinating optical properties that can be maneuvered by controlling their sizes and shapes.[1] Among various types of Ag nanocrystals, nanoplates exhibit exquisite features in the localized surface plasmon resonance (LSPR) owing to an extreme degree of anisotropy in their structure.[2,3] It is well documented that the in-plane LSPR dipole resonance of Ag nanoplates is exceedingly sensitive to the change in morphology – it will be red-shifted with an increase in edge length or blue-shifted with an increase in corner truncation – to encompass peaks over a broad spectral range from visible to infrared.[4–7] Additionally, discrete dipole approximation (DDA) calculations suggest strong electromagnetic fields at the corners of Ag nanoplates and thus remarkable activity for surface-enhanced Raman scattering (SERS), especially when they are arranged in a bowtie structure.[8] Hence, Ag nanoplates offer great potential for an array of applications that leverage their SERS activity for the monitoring of reaction kinetics *in situ*[9–11] and detection of biological or chemical species with high sensitivity.[12–14] Furthermore, when compared with nanospheres and nanowires having the same volume, nanoplates have such larger surface areas, with a strong tendency to form large, ultrathin sheets for potential use as metallic inks in printable electronics.[15,16]

Strategically, the formation of Ag nanoplates can be prepared using a kinetically controlled process, in which the

Y. Yang, Dr. Q. Zhang, L. G. Blackstad, Prof. D. Qin,
School of Materials Science and Engineering
Georgia Institute of Technology
Atlanta, GA, 30332, USA
E-mail: dong.qin@mse.gatech.edu
Y. Yang, Prof. Z.-W. Fu
Department of Materials Science
Fudan University
Shanghai, 200433, P. R. China
X.-L. Zhong, Prof. Z.-Y. Li
Laboratory of Optical Physics
Beijing National Laboratory for Condensed Matter Physics
Institute of Physics
Chinese Academy of Sciences
Beijing, 100190, P. R. China

DOI: 10.1002/smll.201302877

NANO MICRO small

atoms would form plate-like seeds through random hexagonal close packing with the inclusion of stacking faults, followed by their growth into nanoplates.[17] Since the first report on the synthesis of Ag nanoplates using a photo-induced reaction by Mirkin and coworkers,[18] great efforts have been devoted to the development of methods that are based on photochemical reduction,[19–22] thermal decomposition,[23–26] electrochemical reduction,[27] ultrasound-assisted reduction,[28] seed-mediated growth,[29] galvanic replacement,[30] and Ostwald ripening.[31] Most of them involved the use of citrate as a capping agent. Recently, we reported a citrate-free protocol for the synthesis of Ag nanoplates in ethanol with an edge length of 50 nm and a conversion yield approaching 100%.[32] More importantly, when the reaction temperature was above the boiling point of ethanol, the accelerated etching could effectively transform multiple twinned particles (MTPs) into nanoplates. In this case, etching selectively occurred on the high-energy surfaces of MTPs, through which Ag atoms were oxidized to ions. The ions were then reduced back to atoms, leading to the growth of nanoplates at the expense of MTPs. We suspect that the etching should continue on the nanoplates once all the MTPs have disappeared from the reaction system. To this end, a comprehensive understanding of the effects of etching on various facets of Ag nanoplates with different surface free energies would allow us to maneuver the final morphology of the nanoplates. Unfortunately, due to the reducing power of ethanol, we were unable to manipulate the rate and site of etching to see how these parameters would affect the morphology of nanoplates.

In this paper, we report a systematic investigation on the role of etching in the formation of Ag nanoplates during the reduction of $AgNO_3$ by poly(vinyl pyrrolidone) (PVP) in water under a hydrothermal condition. We replaced ethanol with water to eliminate the possible involvement of solvent as a reductant. In our previous work, we found that an inclusion of *ca.* 5% water in ethanol could significantly slow down the reduction rate to generate a smaller number of seeds, leading to the formation of MTPs and nanoplates with larger sizes in the final product.[32] Herein, we performed the reduction of $AgNO_3$ with PVP in DI water at 160 °C under a hydrothermal condition. As expected, the reducing power of PVP in an aqueous solution was significantly weakened as compared with the same reaction in ethanol, leading to the generation of fewer seeds and thereby Ag nanoplates with edge lengths in the range of 100–450 nm. Remarkably, the slower reduction of $AgNO_3$ in an aqueous system allowed us to resolve the role of etching in regulating the formation of Ag nanoplates with different morphologies, which could not be achieved in our previous synthesis with ethanol. We also re-dispersed Ag nanoplates synthesized in water under a hydrothermal condition in ethanol and then subjected them to a solvothermal treatment. Interestingly, the Ag nanoplates with straight edges were transformed into nanoplates with wavy edges and sharp corners during the solvothermal treatment. The ability to generate Ag nanoplates with different edge morphologies allowed us to evaluate their SERS properties. A direct comparison study indicated that nanoplates with wavy edges and sharp corners exhibited the strongest SERS. Our experimental data are supported by the results from finite difference time domain (FDTD) calculations.

2. Results and Discussion

2.1. Quantitative Analysis of the Reduction Process

Compared with previous syntheses under ambient conditions,[23–26] our hydrothermal process at an elevated temperature and induced pressure could significantly shorten the reaction time to 4 h in the generation of Ag triangular nanoplates with straight edges. We were able to monitor the reduction by quenching the standard syntheses after different periods of time and characterizing the products using a number of techniques. Specifically, we used inductively coupled plasma mass spectrometry (ICP-MS) to determine the total amount of Ag in the reaction system (solid plus supernatant) and the content of unreacted Ag^+ ions in the solution after the solid had been removed from the supernatant by high-speed centrifugation. The difference between these two values corresponds to the Ag content in the solid product. Additionally, we used electron microscopy (EM) and UV-vis to characterize the morphology and LSPR properties of the Ag nanoparticles.

Figure 1 shows the UV-vis spectra and ICP-MS data, respectively, of the products obtained at various reaction times up to 6 h at 160 °C. At 0.5 h, no feature was observed in the UV-vis spectrum while the ICP-MS data shows a decrease in Ag^+ concentration from 291 to 239 μM in the solution, indicating that *ca.* 18% of the initially added Ag^+ ions had been reduced into Ag atoms. This result suggests that PVP has a milder reducing power in an aqueous solution than in ethanol, which is consistent with the findings described in previous reports.[32–34] At 1.5 h, we observed a weak LSPR peak at 430 nm in the UV-vis spectrum, indicating the formation of MTPs with relatively small sizes. At 2.5 h, the peak at 430 nm slightly increased in intensity, together with the onset of a weak peak at 560 nm that can be assigned to the in-plane dipole resonance of small Ag nanoplates.[7] As indicated by the ICP-MS data, the concentration of remaining Ag^+ ions was sustained at an average value of 250 μM in the solution from 0.5 to 2.5 h. This result is different from the solvothermal synthesis in ethanol,[32] where the concentration of Ag^+ ions quickly dropped by 90% during the first 0.5 h.

As the reaction progressed to 3.5 h, the peak of MTPs at 430 nm drastically increased in intensity and the dipole peak of Ag nanoplates also significantly increased in intensity with a remarkable red-shift to 1017 nm. A new peak appeared at 337 nm, which can be assigned to the out-of-plane quadrupole resonance of Ag nanoplates. The ICP-MS data also shows a substantial decrease in Ag^+ concentration from 266 to 112 μM during the period of 2.5 to 3.5 h. These results suggest rapid consumption of the remaining Ag^+ ions due to continuous increase in population for the MTPs and fast growth in edge length for the nanoplates. At 4 h, the concentration of Ag^+ ions further declined to 50 μM. The peak of MTPs at 430 nm essentially disappeared and the dipole peak of nanoplates was red-shifted to 1300 nm while their

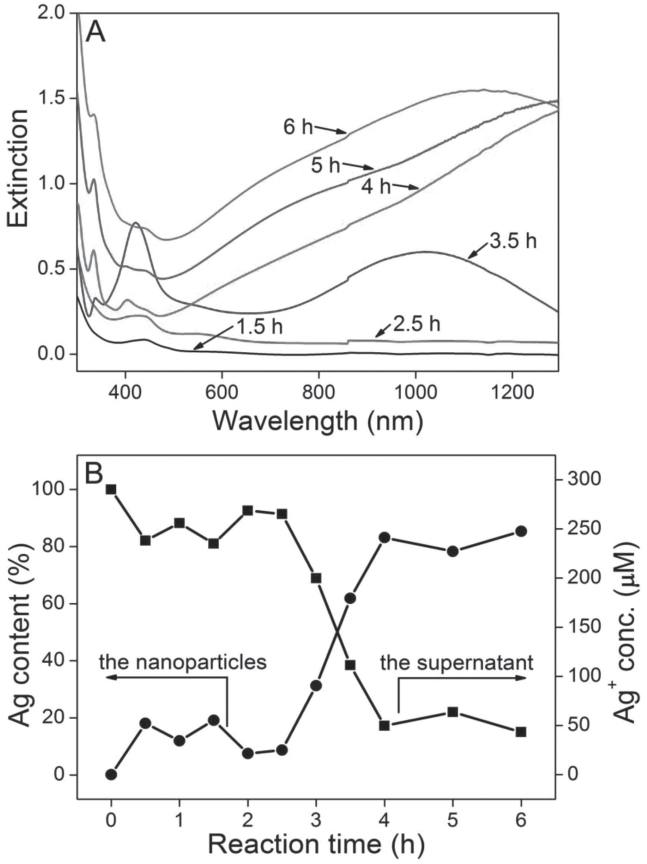

Figure 1. (A) UV-vis spectra of Ag nanoparticles obtained from six standard syntheses quenched at different reaction times; (B) ICP-MS data of the corresponding products (solids and supernatants) together with four additional data points at t = 0, 0.5, 1.0, 2.0, and 3.0 h, showing percentages of the initially added Ag^+ ions that had been converted into Ag nanoparticles (solid) and those remaining in the reaction solutions (supernatant). The Ag^+ concentration only applies to the supernatant.

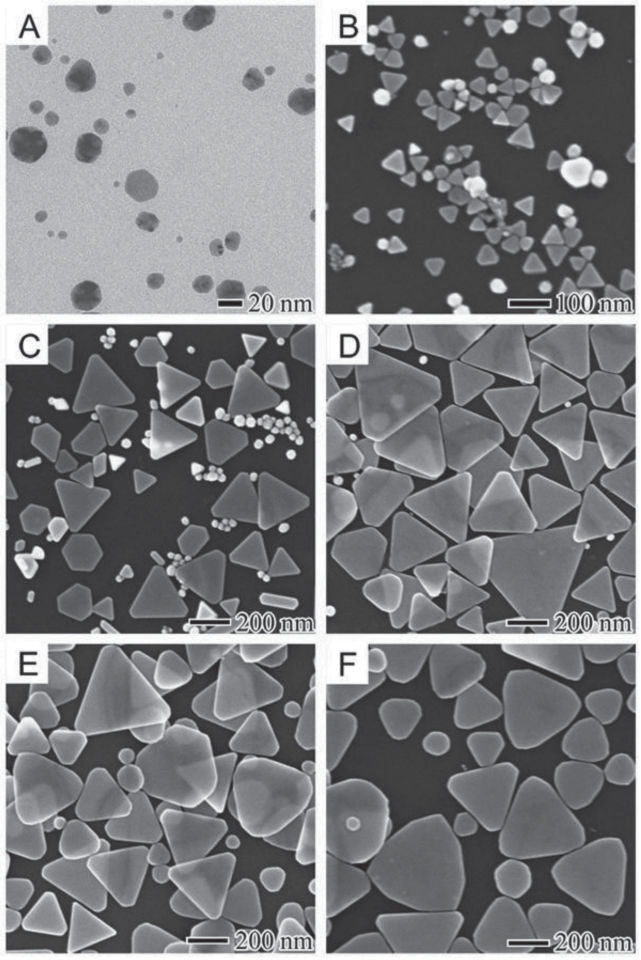

Figure 2. (A) TEM and (B-F) SEM images of Ag nanoparticles obtained from six standard syntheses stopped at different reaction times: (A) 1.5, (B) 2.5, (C) 3.5, (D) 4, (E) 5, and (F) 6 h, respectively. These images were taken form the same samples shown in Figure 1A.

quadrupole peak at 337 nm became much stronger. Taken together, these results indicate efficient transformation from MTPs to nanoplates under the hydrothermal condition, which is similar to our findings for the solvothermal synthesis of Ag nanoplates in ethanol.[32] During this period from 3.5 to 4 h, the Ag^+ concentration in the solution decreased from 112 to 50 μM, suggesting another route for the growth of nanoplates through direct reduction of the remaining Ag^+ ions (*i.e.*, involving no MTPs). This result is different from the solvothermal synthesis in ethanol. As indicated by the UV-vis spectra, there was essentially no MTPs in the solution during the period from 4 to 6 h. Additionally, we observed a blue shift for the dipole peak from 1300 to 1112 nm, suggesting the truncation of sharp corners for the nanoplates due to etching.[35] The etching process should release Ag^+ ions into the solution to cause a slight increase in Ag^+ concentration. However, the concentration of Ag^+ ions remained at a more or less constant level of 50 μM after 4 h. In this case, the Ag^+ ions dissolved from the sharp corners of the nanoplates were reduced by PVP and re-deposited onto the nanoplates without involving additional self-nucleation and growth. It is reasonable to understand this result by assuming that the reduction and oxidation processes had reached equilibrium. At the end, the ICP-MS data confirms that >80% of the originally added Ag^+ ions had been converted into the Ag nanoplates after 6 h of reaction.

The UV-vis and ICP-MS results are consistent with the morphology characterization by EM. **Figure 2** shows electron micrographs of the corresponding solid products collected at different reaction times. The image in Figure 2A indicates the formation of MTPs with an average size larger than 20 nm and small nanoplates with an average size less than 10 nm at 1.5 h into the synthesis. As shown in Figure 2B, MTPs of 36 nm in size and triangular nanoplates with an average edge length of 43 nm were formed at 2.5 h. Figure 2C shows the growth of triangular nanoplates into an edge length of 214 nm, together with an increase in population of MTPs in the course of reaction from 2.5 to 3.5 h. Figure 2D indicates the formation of larger nanoplates with an edge length of 338 nm at 4 h whereas the population of MTPs significantly decreased. Figure 2, E and F, implies the evolution of triangular nanoplates with straight edges into enneahedral nanoplates with curved edges. It is reasonable to understand a broad distribution in edge length from 100 to 450 nm for the Ag nanoplates because nucleation constantly occurred

NANO MICRO small

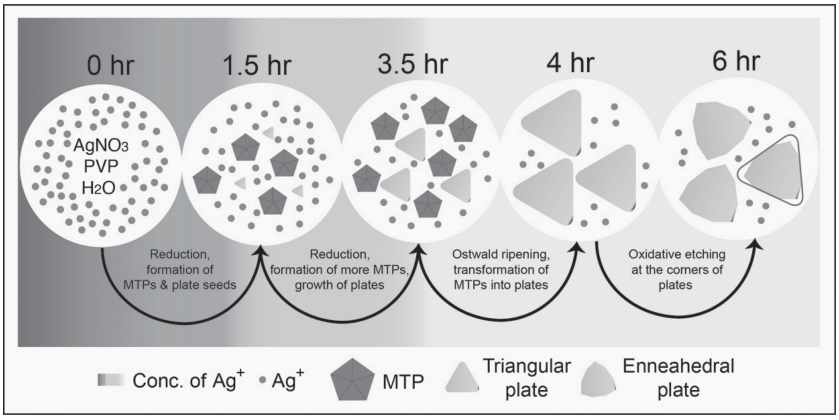

Figure 3. A schematic diagram showing a possible mechanism for the formation of Ag triangular nanoplates with straight edges and enneahedral nanoplates with curved edges during a hydrothermal synthesis.

at different stages of the hydrothermal reaction. However, these nanoplates have a uniform thickness of 17.6 ± 2.5 nm (Figure S1) as measured by atomic force microscopy for the sample shown in Figure 2D.

2.2. Understanding the Role of Etching in the Formation of Ag Nanoplates with Straight, Curved, and Wavy Edges

The UV-vis, ICP-MS, and EM results provide a consistent picture about the reaction process. **Figure 3** schematically illustrates the reaction details and highlights the role of etching in the formation of Ag nanoplates with straight and curved edges. Like the solvothermal synthesis in ethanol, the reduction of Ag^+ ions by PVP in an aqueous solution was a thermodynamically controlled process, in which the majority of the Ag atoms nucleated and grew into MTPs to achieve the lowest total surface energy.[17] In contrast to the solvothermal synthesis with a conversion of 90% in the early stage, the formation of MTPs and small nanoplates only account for a conversion of *ca.* 18%, with the concentration of Ag^+ ions remaining at a high level of *ca.* 239 μM. As the reaction progressed, the formation of MTPs and the growth of nanoplates continuously consumed the Ag^+ ions. As a result, the concentration of Ag^+ ions was further reduced to a level at which MTPs with a higher surface energy became susceptible to the O_2 contained in the reaction vessel. During the period from 3.5 to 4 h, oxidation-assisted Ostwald ripening triggered the quick growth of Ag nanoplates with straight edges at the expense of MTPs. We found that the molar ratio of PVP to $AgNO_3$, [PVP]/[$AgNO_3$], was an important parameter in controlling the formation of nanoplates in the hydrothermal synthesis. For example, at a slower reduction rate corresponding to a [PVP]/[$AgNO_3$] ratio of 5:3, the relatively large MTPs could not be completely transformed into nanoplates (Figure S2). When the [PVP]/[$AgNO_3$] ratio was greater than 10:3, the faster reduction rate favored the formation of MTPs with a smaller size, which facilitated complete transformation into nanoplates with a conversion yield approaching 100%. Upon the depletion of MTPs, the concentration of Ag^+ ions was further reduced to 50 μM, at which selective etching at the corners with higher surface energies started to transform the triangular nanoplates with straight edges into enneahedral nanoplates with curved edges. In this case, the etching at each corner generated two new facets different from those at the edges of the original nanoplates.

We conducted another set of experiments to validate the aforementioned mechanism. Specifically, we followed the standard synthesis to prepare a batch of Ag triangular nanoplates (Figure 2D) by reducing $AgNO_3$ with PVP under hydrothermal reduction at 160 °C for 4 h. The as-obtained sample was further used to perform the three experiments described in **Figure 4**A. When the as-prepared sample was subjected to an additional 5 h of hydrothermal treatment at 160 °C (route I), the triangular nanoplates were transformed into enneahedral nanoplates with a decrease in averaged edge length from 338 nm to 160 nm (Figure 4B).[36] **Figure 5**A shows UV-vis spectra of the as-obtained sample before and after two cycles of washing with DI water and centrifugation. Different from the initial Ag triangular nanoplates, the product shows a peak at 812 nm for the enneahedral nanoplates, together with an LSPR peak at 430 nm due to the presence of MTPs. In this case, since no additional PVP was added into the reaction solution, the triangular nanoplates were transformed into enneahedral plates due to etching at corners, leading to an increase in concentration for the Ag^+ ions. The limited amount of remaining PVP in the reaction was sufficient to promote the formation of small MTPs through self-nucleation. However, since the [PVP]/[$AgNO_3$] ratio was below the threshold of 5:3, the Ag MTPs could not be transformed into nanoplates *via* Ostwald ripening. This argument is consistent with the results shown in Figure S2. It is worth noting that some of the enneahedral plates could be further converted into circular disks due to etching at the corner sites.

In the second experiment, we collected the triangular nanoplates by centrifugation, followed by their dispersion in 10 mL of 1.0 mM PVP aqueous solution. When this suspension was treated under hydrothermal condition at 160 °C for 5 h (route II), the Ag triangular plates were preserved in terms of both morphology and edge length (Figure 4C). This result confirms that PVP plays an essential role as a reducing agent to promote the reduction process, and ultimately hinders the oxidative etching process. With sufficient PVP in the aqueous solution, any dissolved Ag^+ ions from oxidative etching could be reduced back into Ag atoms and then deposited onto the Ag nanoplates.[37] Whereas it was difficult to quantify the growth along lateral and vertical directions, comparison of the SEM images confirmed that this route mainly promoted growth along the lateral directions.

To better understand the role of oxidative etching in the transformation of Ag nanoplates in different solvents, we used ethanol to replace DI water (route III) while all other experimental parameters were kept the same as those described in route II. Interestingly, with sufficient PVP in ethanol, the

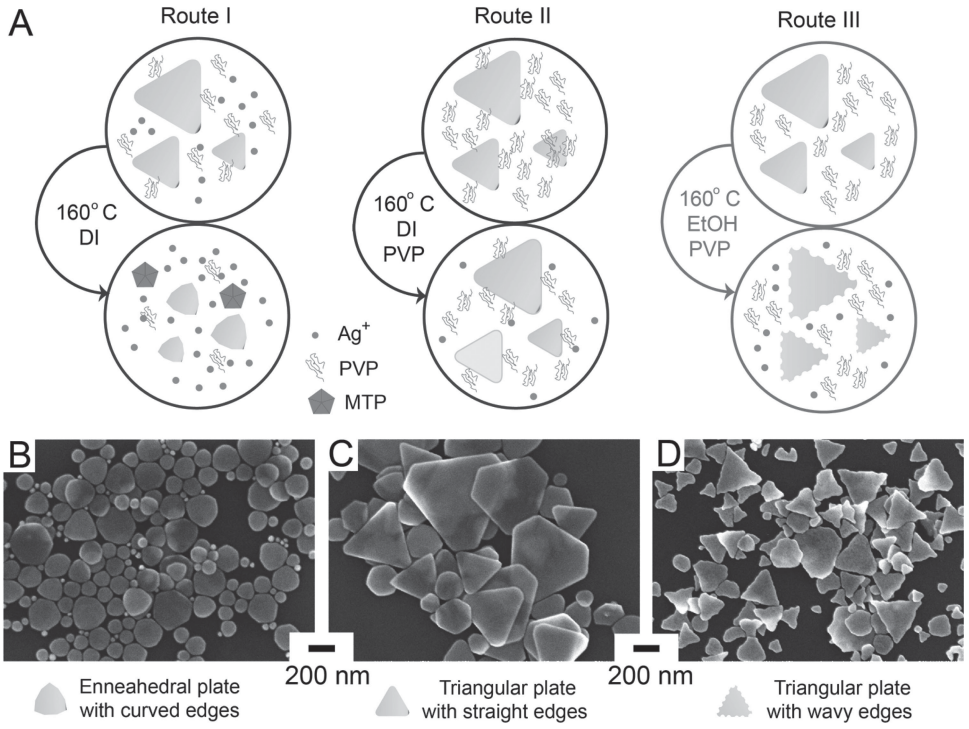

Figure 4. (A) A schematic diagram to elucidate the evolution of Ag triangular plates with straight edges into enneahedral nanoplates and nanoplates with wavy edges in aqueous and ethanol solutions at 160 °C; (B-D) SEM images of (B) enneahedral nanoplates with reduced edge lengths; (C) nanoplates with straight edges and preserved edge length; and (D) Ag nanoplates with wavy edges and reduced edge lengths, respectively.

Ag nanoplates were transformed into a new morphology with sharped corners and wavy edges under a solvothermal condition at 160 °C for 5 h (Figure 4D). In this case, selective etching occurred on the edges rather than at the corners, leading to the formation of triangular nanoplates with wavy edges. Figure 5B shows the UV-vis spectra of the as-obtained sample before and after two cycles of washing with DI water and centrifugation. Without washing and centrifugation, the presence of LSPR peak at 430 nm indicates the formation of MTPs in the transformation process. Upon removal of MTPs by centrifugation, the LSPR shows a weak and broad peak centered around 900 nm, which could be assigned to the in-plane dipole peak of nanoplates. The blue shift of this peak indicates a decrease in edge length. Collectively, our results suggest that oxidative etching of Ag nanoplates occurred on the edges in ethanol under elevated temperature and pressure in the presence of adequate PVP, leading to an increase in the concentration of Ag^+ ions for the formation of MTPs by self-nucleation. To our knowledge, we are the first to observe the etching of Ag nanoplates at the edges to generate nanoplates with wavy edges. As it is anticipated, the structural defect sites on the edges with higher surface energies should become more susceptible to oxidation. Our observations suggest that the {100} facets at the edges were capped more strongly by PVP in DI water than in ethanol, leading to two completely different pathways for selective etching of Ag nanoplates at corners and edges, respectively. It is also worth noting that the wavy nanoplates still have well-preserved sharp corners, indicating the possible growth at the corners of Ag nanoplates in the presence of PVP.

2.3. Comparison of the SERS of Ag Nanoplates with Straight, Curved, and Wavy Edges

It is anticipated that the Ag nanoplates with sharp corners and wavy edges could generate greatly enhanced local electric fields for SERS. To examine the dependence of SERS activity on the morphology, we performed a comparison study using Ag nanoplates (at the same particle concentration) with straight, curved, and wavy edges. **Figure 6** shows the SERS spectra of 1,4-benzenedithiol (1,4-BDT) adsorbed on the surface of these Ag nanoplates using 785 nm laser excitation. The spectra were recorded from aqueous suspensions with the same particle concentration. The peaks at 1564 cm^{-1} and 1078 cm^{-1} can be attributed to the 1,4-BDT signals.[38] In these cases, the peak at 1564 cm^{-1} for nanoplates with wavy and straight edges was 13 and 2 times stronger than that of the nanoplates with curved edges. In the case of Ag nanoplates with wavy edges, the rough edges and sharp corners could serve as hot spots, leading to the strongest SERS signal. In contrast, Ag enneahedral nanoplates with curved edges tend to have round corners, leading to weaker SERS enhancement.

To provide an insight into the strong dependence of SERS on morphology, we performed both far- and near-field calculations for a Ag nanoplate with curved, straight, or wavy edges. Specifically, we used the finite difference time domain (FDTD) method to calculate the extinction spectra for the three types of plates with geometric configurations shown in Figure S2. We assumed that the incident light propagates along the z-axis with polarizations along the x- and

small NANO MICRO

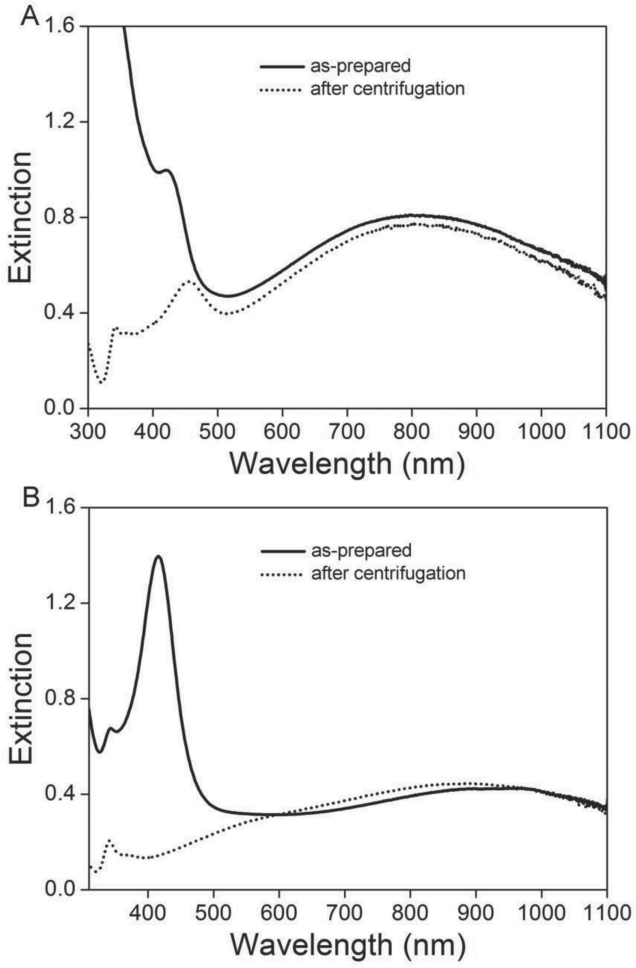

Figure 5. (A) UV-vis spectra of the Ag enneahedral nanoplates shown in Figure 4B before and after two cycles of washing with DI and centrifugation; (B) UV-vis spectra of Ag nanoplates with wavy edges shown in Figure 4D before and after two cycles of washing with DI and centrifugation.

y-axis of the plate, respectively. We used a simulation domain that is 1 mm in each dimension and with a grid size of 2 nm by 2 nm. The perfectly matched layer as boundary condition ensures that electromagnetic waves could be absorbed completely when they reached the simulation boundary.[39] **Figure 7**A compares the calculated extinction spectra. All spectra included in-plane dipole resonances from 600–800 nm and out-of-plane quadrupole resonances around 450 nm, which are consistent with previous calculations for a triangular plate with an edge length of 100 nm.[40] We also found that the in-plane dipole resonance of the nanoplate with wavy edges became significantly broader, together with a shift of the peak position to 800 nm. Figure 7, B and C, shows the E-field enhancement contours with the excitation light (l = 780 nm) polarized along the x- and y-axis, respectively. It is evident that the maximum enhancement occurs at the tips of wavy plates when the in-plane dipole resonance matches the excitation wavelength. These calculations support our experimental observations that the SERS of Ag nanoplates originated from their sharp features at corners and edges and nanoplates with wavy edges were the most active substrates for SERS.

3. Conclusions

We have investigated the role of etching in controlling the formation of Ag nanoplates with different edge morphologies. Specifically, we focused on the reduction of $AgNO_3$ by PVP in an aqueous solution under the hydrothermal condition. At the early stage of a synthesis, both MTPs and plate-like seeds were formed, followed by the increase of MTPs in population and the growth of plate-like seeds in size as more Ag^+ ions were continuously reduced by PVP. When the concentration of Ag^+ ions became sufficiently low, the O_2 present in the reaction vessel would trigger oxidative etching, leading to the quick growth of plate-like seeds into larger triangular plates with straight edges at the expense of MTPs *via* Ostwald ripening. Upon complete consumption of the MTPs, the Ag nanoplates with straight edges were transformed into enneahedral plates with curved edges due to etching at the corner sites. We also demonstrated that etching would occur on the edges of triangular nanoplates to generate wavy structures when they were dispersed in ethanol and subjected to solvothermal treatment. In contrast, nanoplates from the same batch of synthesis were transformed into enneahedral plates under a hydrothermal condition in water due to etching at the corner sites. This finding suggests that the PVP capping in ethanol and DI water could affect the surface energies of edges and corners, resulting in two etching pathways. We further evaluated the SERS properties of Ag nanoplates with different edge morphologies. Our measurements indicate that Ag nanoplates with wavy edges and sharp corners were more active SERS substrates than those

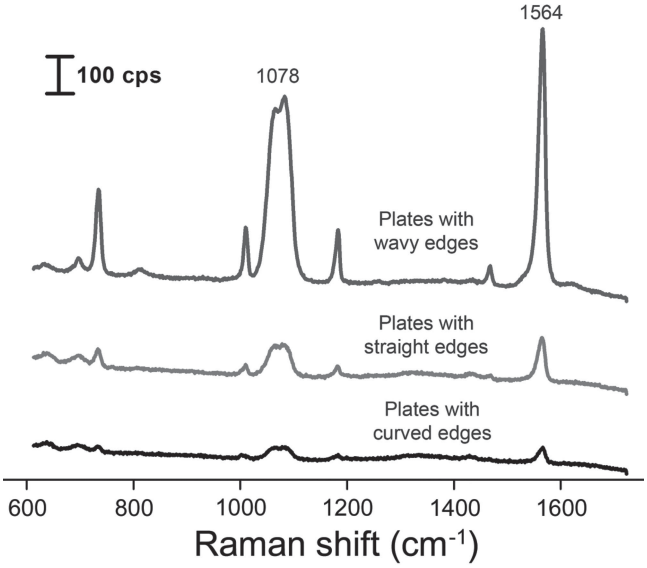

Figure 6. Comparison of SERS spectra at 785 nm laser excitation taken from aqueous suspensions of 1,4-BDT-coated Ag nanoplates with straight edges, curved, and wavy edges, respectively. The peak at 1078 cm^{-1} arises from a combination of the phenyl ring breathing mode, C-H in-plane bending, and C-S stretching, and the peak at 1564 cm^{-1} can be assigned to phenyl ring stretching motion.

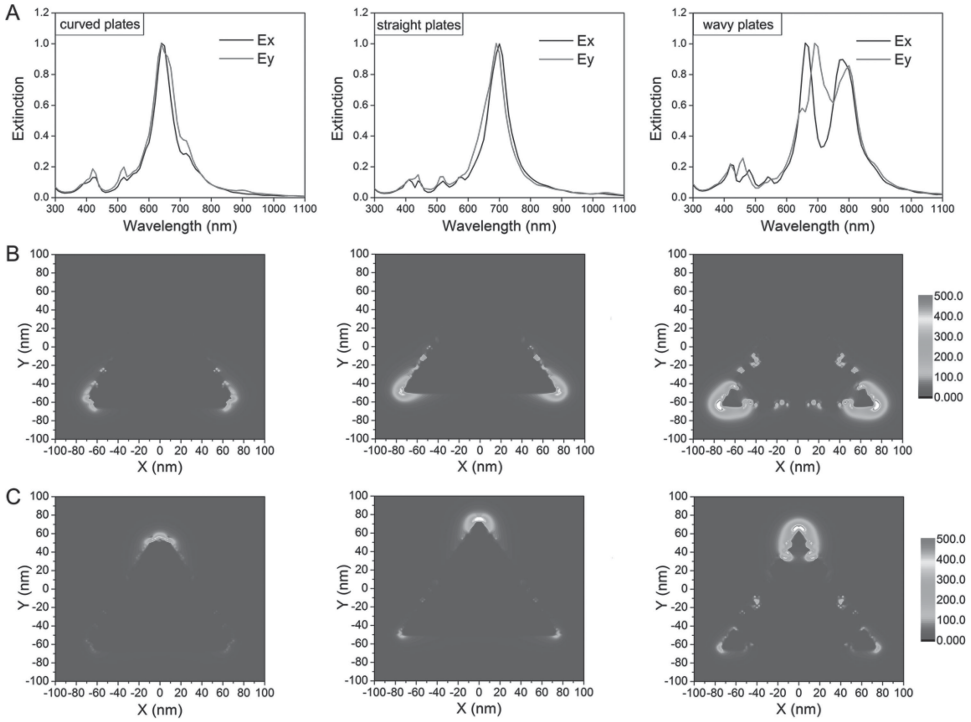

Figure 7. (A) Far-field extinction spectra calculated for a Ag nanoplate with curved, straight, and wavy edges, with an assumption that the incident light propagates along the z-axis and is polarized along the x- and y-axis of a plate (E_x and E_y), respectively; (B) E-field amplitude patterns of a Ag nanoplate with curved, straight, and wavy edges, with E-field along the x-axis (E_x) and an excitation wavelength of 780 nm; (C) E-field amplitude patterns of a Ag nanoplate with curved, straight, and wavy edge, with E-field along y-axis (E_y) and an excitation wavelength of 780 nm.

with straight or curved edges. To understand this difference, we used FDTD to calculate the far-field extinction spectra and near-field E-field contours for nanoplates with curved, straight, and wavy edges, respectively. The calculation results suggest that the wavy plates could promote broadening and a red-shift for the in-plane dipole resonance to match the excitation wavelength of 785 nm, and ultimately generate the strongest E-field enhancement for SERS. The Ag nanoplates with wavy edges embrace a great potential as SERS substrates for both analytical and biomedical applications.

4. Experimental Section

Chemicals: Silver nitrate ($AgNO_3$, 99+%), poly(vinyl pyrrolidone) with an average molecular weight of 29 000 (PVP29K), and ethanol (200 PROOF) were all purchased from Sigma-Aldrich and used as received.

Synthesis of Ag Nanoplates with Straight and Curved Edges: The Ag nanoplates were prepared by heating a mixture of $AgNO_3$ and PVP in DI water at 160 °C in Acid Digestion Vessels (Parr Instrument Company, Catalog Number 4745). In a standard synthesis, $AgNO_3$ and PVP29K were separately dissolved in water at concentrations of 10.0 mM and 1.0 mM (in terms of the average molecular weight of PVP), respectively. Next, the as-prepared PVP solution (10 mL) was added into a Teflon liner, followed by the addition of $AgNO_3$ solution (0.3 mL). The Teflon liner was sealed and placed in the stainless vessel and heated in an oven at 160 °C for 4 h or 6 h to obtain Ag nanoplates with straight or curved edges. Upon completion, the vessel was cooled with water to room temperature prior to dis-assembly. To characterize the sample, 1.5 mL of the as-prepared solution was used to record UV-vis spectra, followed by centrifugation at a speed of 15 000 rpm to separate the solid and supernatant for measuring the Ag contents by ICP-MS. For the preparation of TEM and SEM samples, the particles were collected by centrifugation at 15 000 rpm, washed four times with water to remove excess PVP, re-dispersed in water, dropped on TEM grids or silicon substrates, and then dried under ambient conditions.

Preparation of Ag Nanoplates with Wavy Edges: We initially prepared Ag nanoplates with straight edges using the standard procedure at 160 °C for 4 h. The nanoplates were collected by centrifugation at 15 000 rpm, washed twice with ethanol to remove excess PVP, and then re-dispersed in PVP29K solution (10 mL, 1.0 mM) in ethanol. The newly prepared solution was transferred into a Teflon liner, which was sealed, placed in a stainless vessel, and heated in an oven at 160 °C for 5 h. Upon completion, the vessel was cooled with water to room temperature and the solid was collected by centrifugation at 15,000 rpm, follow by washing with ethanol four times prior to SEM characterization.

Instrumentation and Characterization: The UV-vis spectra were recorded using a Cary 50 spectrometer (Agilent Technologies, Santa Clara, CA). The measurements of Ag contents were performed using ICP-MS (Perkin-Elmer, NexION 300Q). A routine centrifuge (Eppendorf 5430) and a high-speed centrifuge (Beckman Coulter Optima, Max-XP Ultracentrifuge) were used for the collection of solid product from a synthesis and preparation of solid/supernatant samples for ICP-MS, respectively. TEM images were taken using a JEM-1400 microscope (JEOL, Tokyo, Japan) operated at 120 kV. A field-emission scanning electron microscope (Zeiss Ultra 60 FE-SEM) was used to image the Ag nanoparticles with an accelerating voltage of 5 kV.

NANO MICRO small

SERS Measurements: The Ag nanoplates were functionalized with a solution of 1,4-BDT in ethanol (0.6 mM) for 1 h, and then washed with DI water twice. Afterwards, the Ag nanoplates were re-dispersed in DI to achieve a particle concentration of 0.9 nM. The Raman spectra were recorded in the solution phase using a Renishaw in Via Raman spectrometer coupled with a Leica microscope with a 100X objective lens (N.A. = 0.90) in the reflection configuration. We used the excitation wavelength of 785 nm equipped with a holographic notch filter based on a grating of 2400 lines/mm. The Raman signals were collected using deep depletion CCD camera with a laser power of 10 mW and a collection time of 60 s for all samples. The sample cell for SERS was constructed from a poly(dimethyl siloxane) (PDMS) block with a small, punched hole on the surface, which could hold 20 μL of solution. A glass cover slip with a thickness of 170 μm was carefully placed on top of the hole to prevent solvent evaporation and to act as a reference point, from which the focal plane was moved 200 mm into the sample prior to spectrum recording.

Acknowledgements

This work was supported by the start-up funds from Georgia Institute of Technology. Part of the work was performed at the Institute of Electronics and Nanotechnology (IEN) at Georgia Institute of Technology, a member of the National Nanotechnology Infrastructure Network, which was partially supported by NSF (award no. ECS-0335765). Y.Y. was also partially supported by the China Scholarship Council. We thank Zac Combs and Xin Zhao for collecting AFM and ICP-MS data, respectively.

[1] M. Rycenga, C. M. Cobley, J. Zeng, W. Li, C. H. Moran, Q. Zhang, D. Qin, Y. Xia, *Chem. Rev.* **2011**, *111*, 3669.
[2] I. Pastoriza-Santos, L. M. Liz-Marzan, *J. Mater. Chem.* **2008**, *18*, 1724.
[3] J. E. Millstone, S. J. Hurst, G. S. Metraux, J. I. Cutler, C. A. Mirkin, *Small* **2009**, *5*, 646.
[4] X. Jiang, Q. Zeng, A. Yu, *Langmuir* **2007**, *23*, 2218.
[5] B. Tang, J. An, X. Zheng, S. Xu, D. Li, J. Zhou, B. Zhao, W. Xu, *J. Phys. Chem. C* **2008**, *112*, 18361.
[6] K. L. Kelly, E. Coronado, L. L. Zhao, G. C. Schatz, *J. Phys. Chem. B* **2003**, *107*, 668.
[7] A. Brioude, M. P. Pileni, *J. Phys. Chem. B* **2005**, *109*, 23371.
[8] E. Hao, G. C. Schatz, *J. Chem. Phys.* **2004**, *120*, 357.
[9] W. Xu, X. Ling, J. Xiao, M. S. Dresselhaus, J. Kong, H. Xu, Z. Liu, J. Zhang, *Proc. Natl. Acad. Sci. USA* **2012**, *109*, 9281.
[10] K. N. Heck, B. G. Janesko, G. E. Scuseria, N. J. Halas, M. S. Wong, *J. Am. Chem. Soc.* **2008**, *130*, 16592.
[11] Z. Peng, S. A. Freunberger, Y. Chen, P. G. Bruce, *Science* **2012**, *337*, 563.
[12] J. Kneipp, H. Kneipp, K. Kneipp, *Chem. Soc. Rev.* **2008**, *37*, 1052.
[13] J. A. Dieringer, R. B. LettanII, K. A. Scheidt, R. P. Van Duyne, *J. Am. Chem. Soc.* **2007**, *129*, 16249.
[14] E. C. Le Ru, P. G. Etchegoin, *Annu. Rev. Phys. Chem.* **2012**, *63*, 65.
[15] G. D. Moon, G. H. Lim, J. H. Song, M. Shin, T. Yu, B. Lim, U. Jeong, *Adv. Mater.* **2013**, *25*, 2707.
[16] S. B. Walker, J. A. Lewis, *J. Am. Chem. Soc.* **2012**, *134*, 1419.
[17] Y. Xia, Y. Xiong, B. Lim, S. E. Skrabalak, *Angew. Chem. Int. Ed.* **2009**, *48*, 60.
[18] R. Jin, Y. Cao, C. A. Mirkin, K. L. Kelly, G. C. Schatz, J. G. Zheng, *Science* **2001**, *294*, 1901.
[19] R. Jin, Y. C. Cao, E. Hao, G. S. Metraux, G. C. Schatz, C. A. Mirkin, *Nature* **2003**, *425*, 487.
[20] C. Xue, G. S. Metraux, J. E. Millstone, C. A. Mirkin, *J. Am. Chem. Soc.* **2008**, *130*, 8337.
[21] M. Maillard, P. Huang, L. Brus, *Nano Lett.* **2003**, *3*, 1611.
[22] X. Wu, P. L. Redmond, H. Liu, Y. Chen, M. Steigerwald, L. Brus, *J. Am. Chem. Soc.* **2008**, *130*, 9500.
[23] Y. Sun, B. Mayers, Y. Xia, *Nano Lett.* **2003**, *3*, 675.
[24] S. Chen, D. L. Caroll, *Nano. Lett.* **2002**, *2*, 1003.
[25] I. Pastoriza-Santos, L.M. Liz-Marzan, *Nano Lett.* **2002**, *2*, 903.
[26] Q. Zhang, N. Li, J. Goebl, Z. Lu, Y. Yin, *J. Am. Chem. Soc.* **2011**, *133*, 18931.
[27] Y. Sun, G. P. Wiederrecht, *Small* **2007**, *3*, 1964.
[28] L. P. Jiang, S. Xu, J. M. Zhu, J. R. Zhang, J. J. Zhu, H. Y. Chen, *Inorg. Chem.* **2004**, *43*, 5877.
[29] Q. Zhang, Y. Hu, S. Guo, J. Goebl, Y. Yin, *Nano Lett.* **2010**, *10*, 5037.
[30] Y. Lai, W. Pan, D. Zhang, J. Zhan, *Nanoscale* **2011**, *3*, 2134.
[31] S. T. Gentry, S. F. Kendra, M. W. Bezpalko, *J. Phys. Chem. C.* **2011**, *115*, 12736.
[32] Q. Zhang, Y. Yang, J. Li, R. Iurilli, S. Xie, D. Qin, *ACS Appl. Mater. Interf.* **2013**, *5*, 6333.
[33] I. Washio, Y. Xiong, Y. Yin, Y. Xia, *Adv. Mater.* **2006**, *18*, 1745.
[34] M. H. Kim, J. J. Lee, J. B. Lee, K. Y. Choi, *CrystEngComm* **2013**, *15*, 4660.
[35] S. Chen, Z. Fan, D. L. Carroll, *J. Phys. Chem. B* **2002**, *106*, 10777.
[36] Y. Yang, S. Matsubara, L. Xiong, T. Hayakawa, M. Nogami, *J. Phys. Chem. C* **2007**, *111*, 9095.
[37] J. Zeng, X. Xia, M. Rycenga, P. Henneghan, Q. Li, Y. Xia, *Angew. Chem. Int. Ed.* **2011**, *50*, 244.
[38] M. A. Khan, T. P. Hogan, S. Shanker, *J. Raman Spectrosc.* **2008**, *39*, 893.
[39] X. L. Zhong, Z. Y. Li, *J. Phys. Chem. C* **2012**, *116*, 21547.
[40] K. L. Kelly, E. Coronado, L. L. Zhao, G. C. Schatz, *J. Phys. Chem. B* **2003**, *107*, 668.

Received: September 4, 2013
Revised: October 24, 2013
Published online: December 13, 2013